Heliyon 10 (2024) e38648

Contents lists available at ScienceDirect

Heliyon

journal homepage: www.cell.com/heliyon

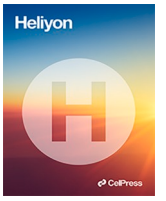

Research article

Shenmai injection improves lipid metabolism in post-myocardial infarction heart failure based on network pharmacology and experimental validation

Jing Yang [a,b], Man Zhao [a], Ting Zeng [b], Lifang Ye [b], Yang Gui [b], Lihong Wang [b,*]

[a] Zhejiang University of Technology, Hangzhou, 310014, China
[b] Department of Cardiovascular Medicine, Zhejiang Provincial People's Hospital, People's Hospital of Hangzhou Medical College, Hangzhou, 310014, China

ARTICLE INFO

Keywords:
Shenmai injection
Post-myocardial infarction heart failure
Lipid metabolism
network pharmacology
Peroxisome proliferator-activated receptor alpha

ABSTRACT

Background: Shenmai injection (SMI), a traditional Chinese medicine formulation derived from the herbal decoction Shenmai Yin, is widely used in treating cardiovascular disorders. This study extensively investigated the effects and mechanisms of action of SMI on lipid metabolism in post-myocardial infarction heart failure (pMIHF).

Methods: Network pharmacology was employed to predict the key targets and associated pathways involved in lipid metabolism for potential SMI treatments in post-myocardial infarction heart failure (pMIHF). Subsequently, a pMIHF mouse model and an ischemia/reperfusion (I/R) cell model were established to delve deeper into and validate the underlying mechanism of action.

Results: We performed network pharmacology analysis, which identified 48 active components in SMI and 201 common gene targets. Subsequent screening using the protein–protein interaction network identified 26 core targets, including interleukin (IL)-6, tumor necrosis factor (TNF)-α, peroxisome proliferator-activated receptor alpha (PPARα), and sirtuin 1 (SIRT1). Based on Gene Ontology and Kyoto Encyclopedia of Genes and Genomes pathway analyses, we predicted that SMI might act on lipid metabolism in pMIHF through the PPARα pathway, a hypothesis supported by the strong binding affinity between this receptor and the active components of SMI, as confirmed via molecular docking. In a left anterior descending artery-ligation mouse model, SMI significantly improved cardiac function, reduced serum free fatty acid levels, decreased inflammatory cell infiltration and myocardial fibrosis, and maintained myocardial mitochondrial morphology. In ischemia-reperfusion (I/R) cells, SMI reduced cell apoptosis, improved mitochondrial membrane potential, and decreased mRNA expression levels of IL-6 and TNF-α, while increasing protein levels of PPARα, SIRT1, and PPARα co-activator-1 alpha (PGC1α).

Conclusion: Collectively, our findings suggest that SMI enhances myocardial lipid metabolism and ameliorates pMIHF by upregulating the PPARα/SIRT1/PGC1α pathway.

* Corresponding author.
E-mail address: wanglhnew@126.com (L. Wang).

https://doi.org/10.1016/j.heliyon.2024.e38648
Received 23 May 2024; Received in revised form 5 September 2024; Accepted 26 September 2024
Available online 5 October 2024

1. Introduction

Myocardial infarction (MI), which is induced by coronary arteriosclerosis, disrupts the local myocardial blood supply, leading to cardiovascular diseases [1]. Clinically, MI is characterized by severe sustained retrosternal chest pain and respiratory distress symptoms. The current therapeutic approaches for MI include essential pharmacotherapy and thrombolysis, which primarily depend on revascularization techniques aimed at restoring myocardial perfusion [2].

The resumption of blood flow to ischemic tissues is beneficial in the short term for alleviating the symptoms of myocardial ischemia and reducing the extent of MI. However, this treatment can exacerbate structural damage to the heart and metabolic dysfunction, and may lead to ischemia-reperfusion (I/R) injury [3], subsequently triggering heart failure. Exploring the functions and regulatory mechanisms involved in the development of heart failure is crucial for the advancement of safer and more effective treatments.

The heart, one of the principal organs in the human body responsible for energy demand and consumption, utilizes substrates such as glucose, fatty acids, and ketone bodies for energy conversion. Fatty acid oxidation is a major source of energy for the heart [4]. However, after MI the energy metabolism substrates in the damaged myocardium undergo a significant shift from fatty acid to glucose metabolism. This metabolic shift results in a critical shortfall in the myocardial energy supply, impacting normal physiological functions and potentially leading to severe consequences such as heart failure [5]. Therefore, improving the efficiency of myocardial lipid metabolism to enhance the myocardial energy status is a promising therapeutic strategy.

Recently, traditional Chinese medicine therapies have emerged as significant alternative treatments for managing post-myocardial infarction heart failure (pMIHF), including shenmai injection (SMI), a herbal formulation widely used clinically [6]. Traditional Chinese medicine TCM theory state that SMI possesses properties that invigorate the "Qi," nourish "Yin," and replenish fluids [7].

Recent studies indicate that SMI can mitigate DOX-induced myocardial damage by suppressing excessive autophagy in myocardial cells [8]. Previous studies have demonstrated that SMI improves energy metabolism, including lipid metabolism, in patients with heart failure and I/R myocardial cells [9,10]. Further investigation is needed to understand the specific mechanisms that SMI has on lipid metabolism. Network pharmacology is a cutting edge technique in traditional Chinese medicine research that enables comprehensive analysis of drug interactions within networks [11].

SMI is a complex, multi-target therapeutic agent that exerts cardioprotective effects by modulating molecular networks. This study utilized network pharmacology to identify therapeutic targets and pathways of SMI for treating pMIHF related to lipid metabolism. The network pharmacology analysis validated the predictive outcomes through in vitro and in vivo experiments.

2. Materials and methods

2.1. Screening of active components and prediction of targets for SMI

Active compounds from *Talinum paniculatum* and *Ophiopogon japonicus*, key components of SMI, were detected through the Traditional Chinese Medicine Systems Pharmacology (TCMSP, https://old.tcmsp-e.com/tcmsp.php) [12]) and Encyclopedia of Traditional Chinese Medicine (ETCM) (http://www.tcmip.cn/ETCM/) [13] databases. The selection criterion used was oral bioavailability (OB) $\geq$ 30 %.

These compounds were further screened using the SwissADME database (http://www.swissadme.ch/) [14] for high gastrointestinal absorption and drug-likeness to identify the effective components in SMI. The compounds were subsequently assessed using the Swiss Target Prediction database with a "Probability >0" filter to determine drug action targets. The identified targets were deduplicated, and their protein identifications (IDs) were retrieved from the UniProt database (https://www.uniprot.org/).

2.2. Screening of targets for pMIHF

Disease targets were identified and filtered using the keywords "post-myocardial infarction heart failure" and "myocardial ischemia-reperfusion injury" in the DisGeNET (https://www.disgenet.org/) [15] and GeneCards (https://www.genecards.org/) [16] databases. The redundant targets were eliminated and gene names were normalized in the UniProt database.

2.3. Construction of pMIHF-target-active ingredient network

Using a Venn diagram (https://www.bioinformatics.com.cn/) [17], the drug action targets of SMI were overlaid with the disease targets of pMIHF to identify potential action targets. A corresponding Venn diagram was generated and the resulting data was then used to construct an interaction network, "pMIHF-target-active ingredient," using the Cytoscape 3.9.1 program. The significance of the network nodes was assessed by analyzing their degree values using topological analysis.

2.4. Construction of protein–protein interaction (PPI) network

Data on potential action targets for SMI in treating pMIHF were submitted to the Search Tool for the Retrieval of Interacting Genes/Proteins (STRING, https://www.string-db.org/) database [18]. Furthermore, *Homo sapiens* was the selected term to generate a PPI network. After importing PPI data into Cytoscape 3.9.1, the core targets were determined and a parameter analysis was carried out using the network analyzer tool. The core target data were re-uploaded to STRING with the confidence level adjusted to "medium confidence = 0.4," generating a PPI core network (PPICN) for SMI treatment of pMIHF.

2.5. Gene Ontology (GO) and Kyoto Encyclopedia of genes and Genomes (KEGG) enrichment analysis

Core targets were analyzed using the Database for Annotation, Visualization and Integrated Discovery (DAVID) database (https://david.ncifcrf.gov/) [19] for GO and KEGG pathway enrichment, with the significance level set at a P-value <0.01. This analysis predicted the potential mechanisms of action of SMI in the treatment of pMIHF. The results were visualized and analyzed using the Weisheng Xin platform.

2.6. Molecular docking validation

The GO and KEGG analyses identified peroxisome proliferator-activated receptor alpha (PPARα) as a key target for the effects of SMI on lipid metabolism in treating pMIHF. The top five active components of SMI were selected, and their protein structures were retrieved from the Protein Data Bank (PDB) database (https://www.rcsb.org/). These components were subjected to molecular docking with PPARα using AutoDock to assess interaction extents via free binding energies. The interactions were visualized and analyzed using PyMOL software.

2.7. Preparation of SMI and fenofibrate

SMI (50 ml, approval number: Z33020019) was sourced from Zhengda Qingchunbao Pharmaceutical Co., Ltd. (Hangzhou, China). The PPARα agonist fenofibrate ($C_{20}H_{21}ClO_4$, purity $\geq$99.7 %) was procured from MedChemExpress (NJ, USA) and used as a positive control. For the in vivo studies, fenofibrate was solubilized in corn oil whereas for the in vitro studies, after dissolving in dimethyl sulfoxide, it was further diluted to the working concentration in the culture medium.

2.8. Animals

In this investigation, male C57BL/6 specific pathogen-free (SPF) grade mice aged eight weeks were employed. Jiangsu Jicui Yaokang Biotechnology Co., Ltd. (Nanjing, China, Certificate No.: SCXK(Su)2023-0009) provided 40 mice in total, each weighing 23 $\pm$ 2 g. The mice were kept at the Zhejiang Provincial People's Hospital Experimental Animal Center. All procedures were approved by the Institutional Animal Care and Use Committee (IACUC) of Zhejiang Provincial People's Hospital (approval number: 2023030815364069742 4), following the National Institutes of Health (NIH) guidelines. The mice underwent left anterior descending (LAD) coronary artery ligation in order to create the pMIHF model [20]. A needle was inserted approximately 2 mm from the lower edge of the left atrial appendage of the mouse, transversely inserted, and quickly ligated. The naked eye observation revealed a white and ischemic ligation site and apical tissue. Electrocardiography was performed on the mouse 24 h post-operation, showing the appearance of ST segment elevation, indicating successful establishment of the model. Following ligation, the mice were housed for 1 week, then randomized into the following four groups (n = 10 each): model (i.p., 0.9 % sodium chloride [NaCl], 2.5 ml kg^{-1}), SMI (i.p., 2.5 ml kg^{-1}), fenofibrate group (p.o., 100 mg kg^{-1}), and sham (i.p., 0.9 % NaCl, 2.5 ml kg^{-1}, without LAD ligation). SMI and fenofibrate dosages were determined by reviewing other research [21,22], and the medication was administered daily for 3 weeks.After the experiment, the mice were sacrificed by cervical dislocation.

2.9. Cardiac function assessment

Three weeks after drug administration, echocardiography was performed to assess the cardiac function in all the experimental groups. The parameters measured were the left ventricular internal diameter in diastole (LVIDd) and systole (LVIDs), ejection fraction (EF), and fractional shortening (FS). The average measurements of three cardiac cycles was calculated to ensure accuracy and consistency.

2.10. Assessment of myocardial injury biomarkers and free fatty acid (FFA) levels

Peripheral blood serum samples were collected for analysis using detection kits (Jinhengnuo, Hangzhou, China) to measure the concentrations of myocardial injury biomarkers, including lactate dehydrogenase (LDH), creatine kinase (CK), and its isoenzyme, CK-MB, were measured. Additionally, the levels of FFA in the peripheral serum were quantified.

2.11. Morphometric analysis

Mouse left ventricular myocardial tissue samples were fixed with 4 % paraformaldehyde, embedded in paraffin, and sectioned for histological analysis. Hematoxylin and eosin staining was used to evaluate myocardial inflammatory infiltration, while Masson's trichrome staining was employed to assess myocardial fibrosis. Tissue samples for ultrastructural analysis were fixed in electron microscope fixative, dehydrated, embedded in acetone and embedding agent, stained with 2 % uranyl acetate and lead citrate, and subsequently examined using an electron microscope to observe the mitochondrial structure.

2.12. Cell culture

H9C2 ventricular myocardial cells from rat embryos were procured from Meisen Cell Technology Co., Ltd. (Hangzhou, China) and cultured in DMEM/high glucose containing 10 % FBS, 100 U/ml penicillin and 0.1 mg/ml streptomycin. The cells were incubated at 37 °C in an atmosphere of 5 % carbon dioxide (CO_2) and subcultured when they achieved 70–80 % confluence to maintain optimal growth.

2.13. Construction of I/R injury model

Cells in the logarithmic growth phase were cultured for 24 h and then exposed to hypoxia for 2 h in a chamber. Then, the medium was refreshed, and the cells were reoxygenated at 37 °C for 1, 3, and 6 h. Finally, the cell viability was assessed using the cell counting kit-8 (CCK8, Beyotime, Shanghai, China) assay to optimize the conditions for the I/R model.

2.14. Concentration determination for SMI

Cells in logarithmic growth were cultured for 24 h and divided into the control-SMI and I/R-SMI groups, that were treated with SMI at concentrations of 0, 0.5, 1, 5, 10, and 25 μl/ml. The I/R-SMI group was subjected to established I/R conditions. Cell viability was assessed using CCK8 assay to determine the optimal SMI concentration.

2.15. Cell apoptosis

H9C2 cardiomyocytes were assigned to the following four groups: Control, I/R model, I/R + SMI (5 μl/ml), and I/R + fenofibrate (10 μM/mL), cells and culture medium were collected from each group. Apoptosis was assessed with FITC Annexin V Apoptosis Detection Kit I (BD, USA). and flow cytometry was immediately conducted using NovoCyte Quanteon Flow Cytometer (2010097, Agilent, USA).

2.16. Assessment of mitochondrial membrane potential

The mitochondrial membrane potential of the live cells was measured using a JC-1 assay kit (Beyotime, Shanghai, China). The cells were examined under a fluorescence microscope (EVOSM7000, Thermo, USA).

2.17. Real-time quantitative polymerase chain reaction (RT-qPCR) analysis

Total RNA was extracted from cells using TRIzol, followed by cDNA extraction with a reverse transcription kit.(AG, Changsha, China). The cDNA-SYBR reaction mixture (AG, Changsha, China) was then quantitatively amplified using the fluorescence quantitative PCR system (ABI7500, Thermo, USA). The primer sequences used are listed in Table 1.

2.18. Western blot analysis

After collecting the cells, they were lysed in pre-cooled RIPA lysis buffer (Beyotime, Shanghai, China) supplemented with 1 % protein phosphate inhibitor(Beyotime, Shanghai, China). The protein concentration was determined using a BCA kit (Thermo, USA). Subsequently, protein electrophoresis was performed on a 10 % SDS-PAGE gel, followed by transfer of the proteins to a PVDF

Table 1
Primer sequences for RT-qPCR.

Primer name	Primer sequence (5'-3')
BAX-Forward	TGGGGCTTGTGAGGTGTATT
BAX-Reverse	GATGACAGAGAAGGGCGGAC
BCL2-Forward	GAGTTCGGTGGGGTCATGTG
BCL2-Reverse	AGGTATGCACCCAGAGTGATG
IL6-Forward	AGTTGCCTTCTTGGGACTGA
IL6-Reverse	ACTGGTCTGTTGTGGGTGGT
TNFα-Forward	GGCGTGTTCATCCGTTCTC
TNFα-Reverse	CTTCAGCGTCTCGTGTGTTTCT
PPARα-Forward	GGCAATGCACTGAACATCGAG
PPARα-Reverse	GCCGAATAGTTCGCCGAAAG
SIRT1-Forward	TCGTGGAGACATTTTTAATCAGG
SIRT1-Reverse	GCTTCATGATGGCAAGTGG
PGC1α-Forward	GAATGCAGCGCTCTTAGC
PGC1α-Reverse	GCTTTTGCTGTTGACAAATG
Actin-Forward	ACCCCGTGCTGCTGACCGAG
Actin-Reverse	TCCCGGCCAGCCAGGTCCA

membrane at 300 mA. The membrane was then blocked with 5 % skim milk powder and incubated with primary antibody overnight at 4 °C. After incubation with the secondary antibody at room temperature, the protein bands were visualized using Image Lab software and further analyzed using ImageJ software.The antibodies were as follows: anti-PPARα antibody (66826-1-lg, Proteintch, China); Anti-SIRT1 antibody (13161-1-AP, Proteintch, China); Anti-PGC1α antibody (66369-1-lg, Proteintch, China); Anti-TUBULIN antibody (10094-1-AP, Proteintch, China).

2.19. Statistical analysis

The experimental data were expressed as means ± SD and group differences were analyzed using a one-way analysis of variance (ANOVA) performed using the GraphPad Prism 8 software. Statistical significance was set at $P < 0.05$.

3. Results

3.1. Active components and targets of SMI

Based on data retrieved from the TCMSP and ETCM databases, 115 active components associated with SMI were identified, including 75 and 40 components from *T. paniculatum* and *O. japonicus*, respectively. Further screening using the Swiss ADME database revealed 24 active components each in *T. paniculatum* and *O. japonicus* (Tables 2 and 3, respectively). Subsequently, these components were imported into the Swiss Target Prediction database where 616 potential SMI drug targets were identified (Supplementary Table 1) (see Table 4).

3.2. Screening of potential targets for activity of SMI in pMIHF

GeneCards and DisGeNET databases were searched and we identified 710 and 756 pMIHF disease targets, respectively. After removing duplicates, a consolidated total of 1051 unique pMIHF disease targets were obtained. These targets along with the drug action targets for SMI were imported into the microbioinformatics platform for further analysis. After creating a Venn diagram to show the overlap, 201 intersecting targets that could be used as SMI therapeutic targets for the treatment of pMIHF were found (Fig. 1A).

3.3. Construction and analysis of pMIHF–target–active ingredient network

We used the Cytoscape 3.9.1 software to visualized the interactions between 48 effective active components and 201 potential action targets, which finally enabled the construction of a "pMIHF–target–active ingredient" network diagram (Fig. 1B). This intricate

Table 2
Active ingredients of *Talinum paniculatum*.

NO.	Pubchem ID	Compound	GI absorption	Druglikeness
1	9898279	Ginsenoside Rb1	high	5
2	12592	Tetracosane	high	4
3	97032059	alpha-Santalene	high	4
4	22169126	Alpha-Farnesene	high	4
5	94164	Pentadecanoate	high	4
6	91746597	20R-Ginsenoside Rg2	high	4
7	75412551	(1aR,4R,4aR,7R,7aS,7bS)-1,1,4,7-Tetramethyldecahydro-1H-cyclopropa(e)azulen-4-ol	high	4
8	5281516	(1aS,4aS,7S,7aR,7bS)-1,1,7-trimethyl-4-methylidene-1a,2,3,4a,5,6,7a,7b-octahydrocyclopropa(h) azulen-7-ol	high	4
9	8369	Palmitic Acid	high	3
10	441923	Maltol	high	3
11	138114286	Piperonal	high	3
12	8438	2,3-Dihydrobenzofuran	high	3
13	11005	Myristic Acid	high	3
14	15560252	Ginsenoside Rg1	high	3
15	85044013	2-Isopropenyl-1-methyl-4-(1-methylethylidene)-1-vinylcyclohexane	high	3
16	985	(−)-Isolongifolene	high	3
17	10329	beta-Guaiene	high	3
18	11127402	Ginsenoside Rs1	high	3
19	6432312	(5S,8R,9S,10R,13S,14R,17R)-17-((2R)-2-hydroxy-6-methylhept-5-en-2-yl)-4,4,8,10,14-pentamethyl-2,3,5,6,7,9,11,12,13,15,16,17-dodecahydro-1H-cyclopenta(a))phenanthrene-3,6,12-triol	high	3
20	145706029	2,2′-Methylenebis(4-ethyl-6-tert-butylphenol)	high	2
21	3086007	Ginsenosides	high	2
22	91746456	1-Heptadecene-4,6-diyne-3,9,10-triol	high	2
23	6928	(1aS,4aS,7aS,7bR)-1,1,7-trimethyl-4-methylidene-2,3,4a,5,6,7,7a,7b-octahydro-1aH-cyclopropa(e) azulene	high	2
24	10540577	(8R,10R,14R)-17-((2R)-2-hydroxy-6-methylhept-5-en-2-yl)-4,4,8,10,14-pentamethyl-2,3,5,6,7,9,11,12,13,15,16,17-dodecahydro-1H-cyclopenta(a)phenanthrene-3,12-diol	high	2

Table 3
Active ingredients of *Ophiopogon japonicus*.

NO.	Pubchem ID	Compound	GI absorption	Druglikeness
1	5280537	N-Trans-feruloyltramine	high	5
2	5316797	ophiopogonanone E	high	5
3	5317207	6-Aldehydo-isoophiopogonone A	high	5
4	5317212	6-Aldehydoisoophiopogonone B	high	5
5	5318201	Ophiopogonanone F	high	5
6	5372945	Paprazine	high	5
7	5374699	Jasmolone	high	5
8	9996586	Ophiopogonanone A	high	5
9	10087732	Ophiopogonone A	high	5
10	10246745	5,7-Dihydroxy-6-methyl-3-((4-hydroxy-1,3-benzodioxol-5-yl)methyl)chromone	high	5
11	10871974	CID 10871974	high	5
12	11003181	Ophiopogonanone D	high	5
13	11142766	Ophiopogonone C	high	5
14	11185637	(S)-p-Coumaroyloctopamine	high	5
15	46886723	Methylophiopogonanone B	high	5
16	53466984	Methylophiopogonanone A	high	5
17	53467849	(3R)-5,7-dihydroxy-3-((4-hydroxy-3-methoxyphenyl)methyl)-6,8-dimethyl-2,3-dihydrochromen-4-one	high	5
18	76036450	2,3-Dihydro-3-(4-methoxybenzyl)-5,7-dihydroxy-6-methyl-4H-1-benzopyran-4-one	high	5
19	72607	2-((3r,5s,8r)-3,8-Dimethyl-1,2,3,4,5,6,7,8-octahydroazulen-5-yl)propan-2-ol	high	4
20	441893	Ruscogenin	high	4
21	753	Glycerin	high	3
22	2537	Camphor	high	3
23	6549	Linalool	high	3
24	11230	4-Terpineol	high	3

Table 4
The minimum binding energies of PPARα with effective active components.

Ingredients	Compound	minimum binding energy/(kcal/mol)
T. paniculatum	ginsenoside Rb1	−7.5
O. japonicus	jasmolone	−6.4
O. japonicus	2,3-dihydro-3-(4-methoxybenzyl)-5,7-dihydroxy-6-methyl-4H-1-benzopyran-4-one	−8.4
T. paniculatum	γ-elemene	−5.9
T. paniculatum	ginsenoside Rg1	−6.9

network comprised 250 nodes and 926 edges. Degree values were used to quantify the relationships between the components and the relevant action targets. The top 5 effective components ranked by their degree values are listed in Supplementary Table 2.

3.4. Construction of PPI network and selection of core action targets

We utilized the STRING database to import potential targets and create the protein-protein interaction (PPI) network (Fig. 2A). Our analysis revealed that the PPI network comprised 190 nodes and 1068 edges. Subsequent topological analysis using Cytoscape 3.9.1 software indicated that the average degree, betweenness, and closeness centrality values were 11.242, 367.357, and 0.202, respectively. Nodes exceeding the average values of these three parameters were selected as core action targets (Fig. 2B). The 26 core proteins were then imported into the STRING database to generate the PPI-core network (PPI-CN), depicted in Fig. 2C.

3.5. GO and KEGG functional enrichment analysis

we performed GO and KEGG enrichment analyses of 26 main action targets. 434 entries were found in the GO analysis; of these, 31, 347, and 56 had to do with biological processes, cellular components, and molecular activities, respectively. Fig. 2D–F shows the top 20 targets ranked by degree within these categories. Furthermore, the KEGG pathway analysis identified 146 signaling pathways. We selected the top 20 pathways most closely related to pMIHF for the bubble chart analysis (Fig. 2G). Based on our findings, we further explored lipid metabolism-related pathways. The pathways associated with lipid metabolism and atherosclerosis predominantly included core targets such as PPARα, SIRT1, IL6, TNFα, and BCL2. Based on the results of core target protein and KEGG pathway analyses, we hypothesize that PPARα may be a central target in lipid metabolism for the action of SMI in the treatment of pMIHF.

3.6. Molecular docking validation

The results of the molecular docking analysis of the minimum binding energies of PPARα with various effective active components are presented in Table 3 and Fig. 3A–E. The results show that values of the five most closely related effective active components were −7.5, −6.4, −8.4, −5.9, and −6.9 kcal/mol, indicating that they all exhibited high binding activity. This suggests a significant

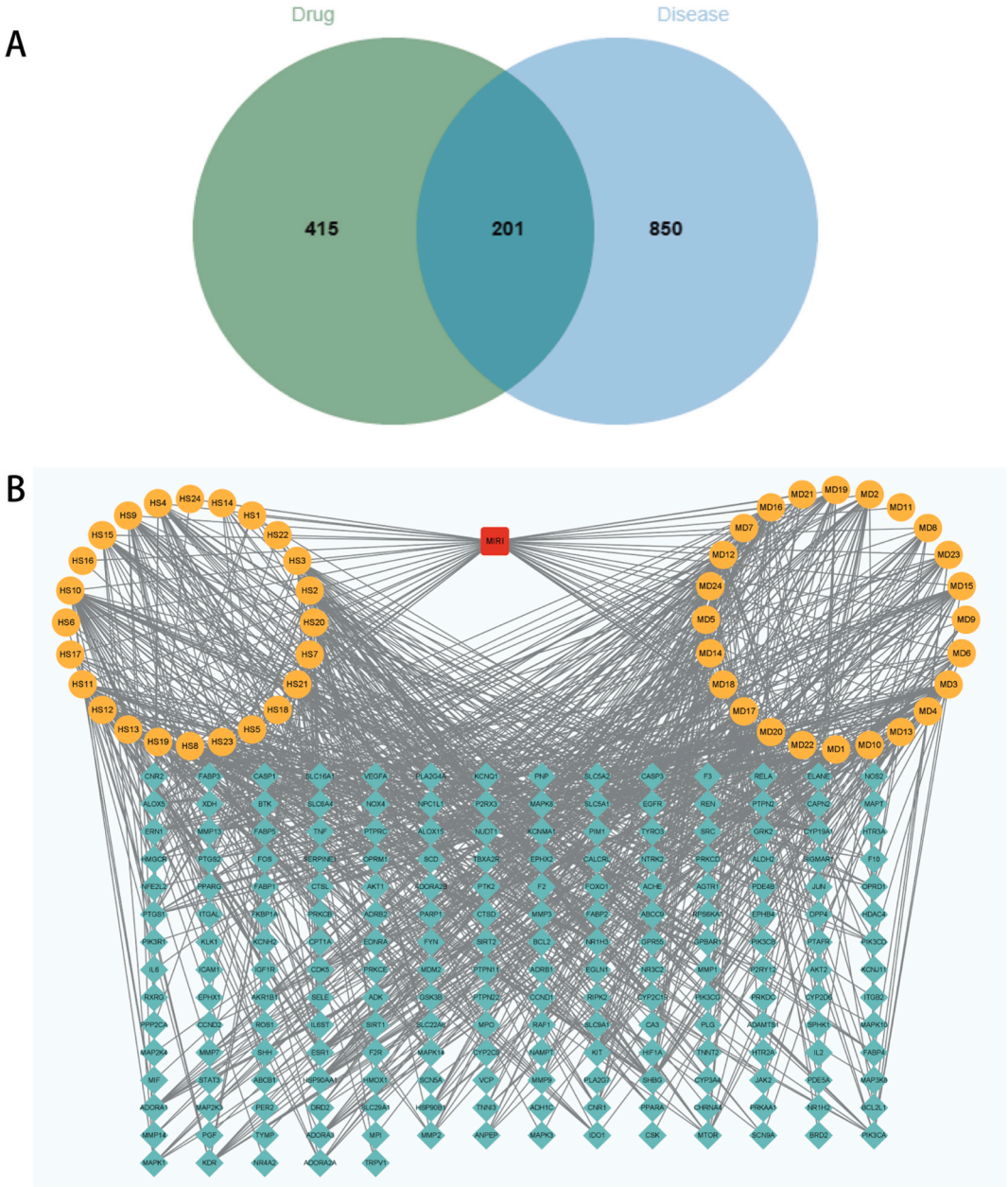

Fig. 1. pMIHF–target–active ingredient network. (A) Venn diagram for overlap analysis of SMI and pMIHF targets. There were 201 relevant overlapping targets. (B) pMIHF–target–active ingredient network. Red, orange, and green node represents pMIHF, targets, and ingredients, respectively.

interaction between PPARα and SMI in pMIHF. Fig. 3 displays the binding sites and hydrogen bonds between top 5 effective active components and PPARα.

3.7. SMI treatment in LAD mice

The specific method for establishing the LAD mouse model is shown in Fig. 4A. Following LAD ligation, abnormal changes were observed in the electrocardiograms of the mice, with a significant elevation of the ST segment (As shown by the red arrow, Fig. 4B), appearance of pathological Q waves, and noticeable widening of the QST complex (As shown by the green arrow, Fig. 4B). As shown in Fig. 4C, the myocardial volume of the mice in the model group was visibly larger than that of mice in the sham, SMI, and fenofibrate groups. Moreover, the body weight gain results indicated that the growth rate of the model group was significantly higher than that in the other three groups, reaching growth rates of 1.076 % and 1.13 % in the second and third weeks of the experiment, respectively

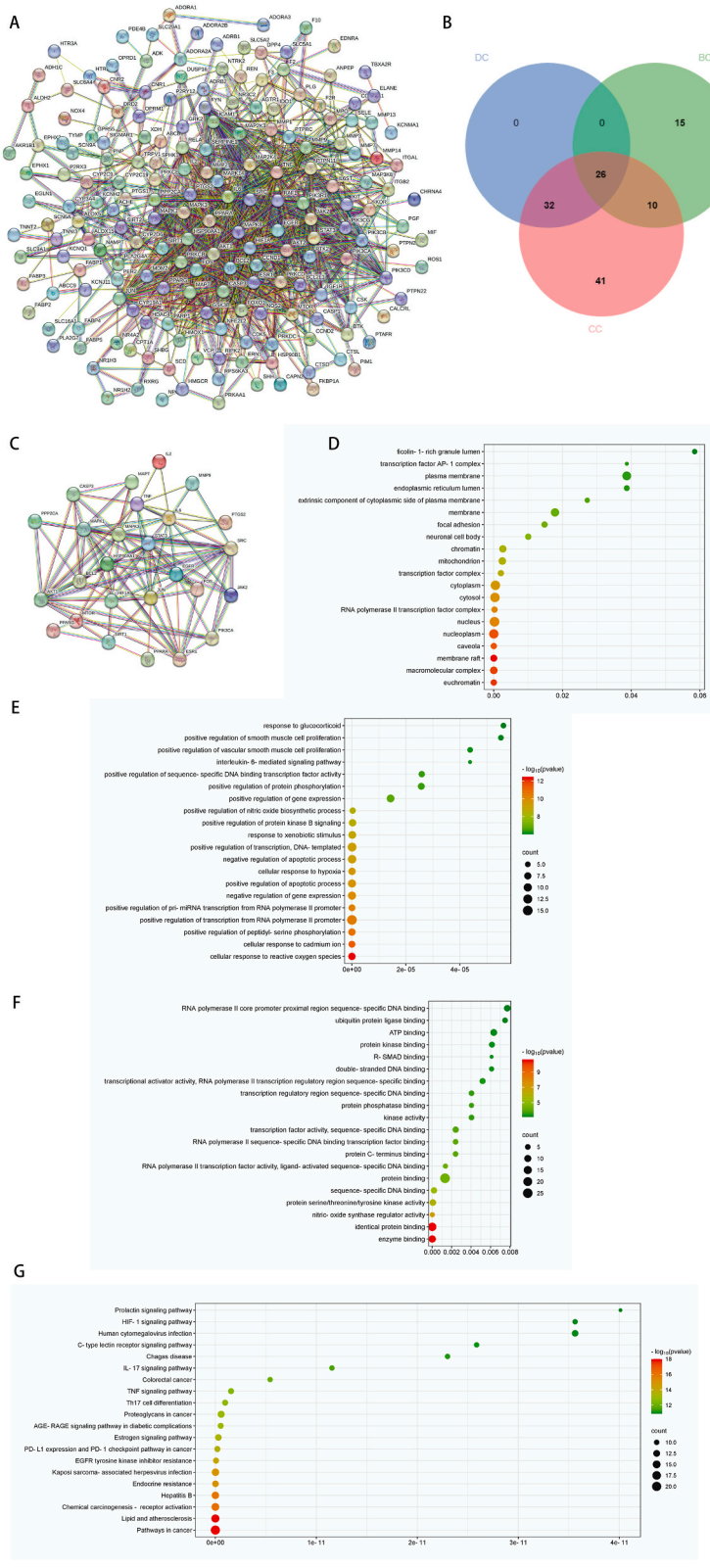

(caption on next page)

Fig. 2. Protein–protein interaction network and enrichment analysis. (A) PPI network was constructed by STRING database. (B) Venn diagram of overlap analysis of degree centrality–closeness centrality– betweenness centrality. (C) PPICN network of 26 key targets. Top 20 terms of GO- (D) biological processes, (E) cellular components, and (F) molecular functions. (G) Bar graph of KEGG enrichment analysis for 26 key targets (top 20 results).

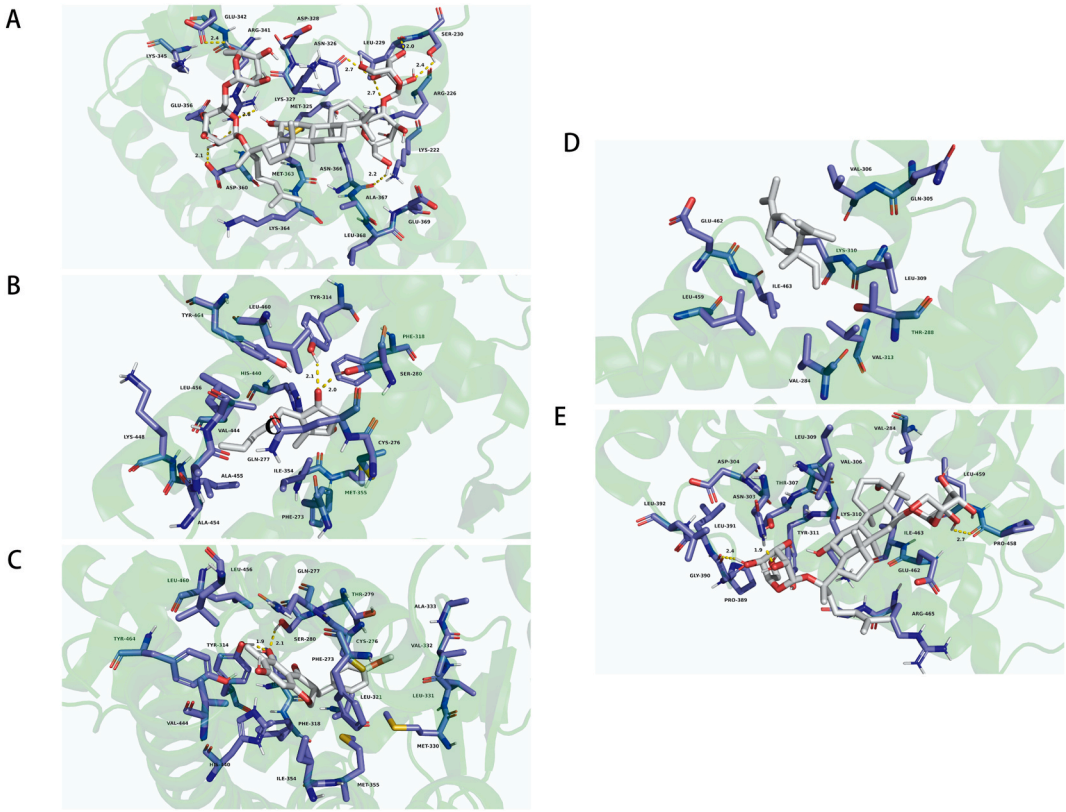

Fig. 3. Binding sites and hydrogen bonds of PPARα with (A) ginsenoside Rb1, (B) jasmolone, (C) 2,3-dihydro-3-(4-methoxybenzyl)-5,7-dihydroxy-6-methyl-4H-1-benzopyran-4-one, (D) γ-elemene, and (E) ginsenoside Rg1.

(Fig. 4D).

Additionally, the results comparing the heart weight to body weight ratio (HW/BW) among the groups showed that the values for the sham, model, SMI, and fenofibrate groups were 4.557 ± 0.178, 8.106 ± 1.011, 6.041 ± 0.877, and 7.284 ± 1.136, respectively. Compared to the Sham group, the HW/BW ratio of the model group was significantly increased and was the highest among all the groups, followed by that of the fenofibrate group. The HW/BW ratio of the SMI group was lower than that of the model group (Fig. 4E).

3.8. Effect of SMI on cardiac function in LAD mice

The echocardiographic results (Fig. 5A–E) showed that the model group exhibited significant lower EF and FS than the sham group. In contrast, the SMI group showed relative improvements in EF and FS compared to the model group (Fig. 5D and E). Regarding the cardiac structure, compared to the sham group, the LVIDs and LVIDd in the model group were significantly increased. However, both the LVIDs and LVIDd were lower in the SMI group than they were in the model group. The effects of fenofibrate were similar to those of SMI, but there was no significant difference in the fractional shortening compared to the model group (Fig. 5B and C).

3.9. Effects of SMI on myocardial markers and FFA levels in LAD mice

Analysis of serum myocardial markers in the mice (Fig. 5F–H) showed that compared to the sham group, the levels of LDH, CK-MB, and CK were significantly elevated in the model group. In contrast, compared with the model group, the serum LDH, CK-MB, and CK levels of the SMI group were significantly reduced. Furthermore, the model group exhibited significantly lower FFA levels than those of the sham group, whereas levels in the SMI group were significantly higher than those in the model group were (Fig. 5I).

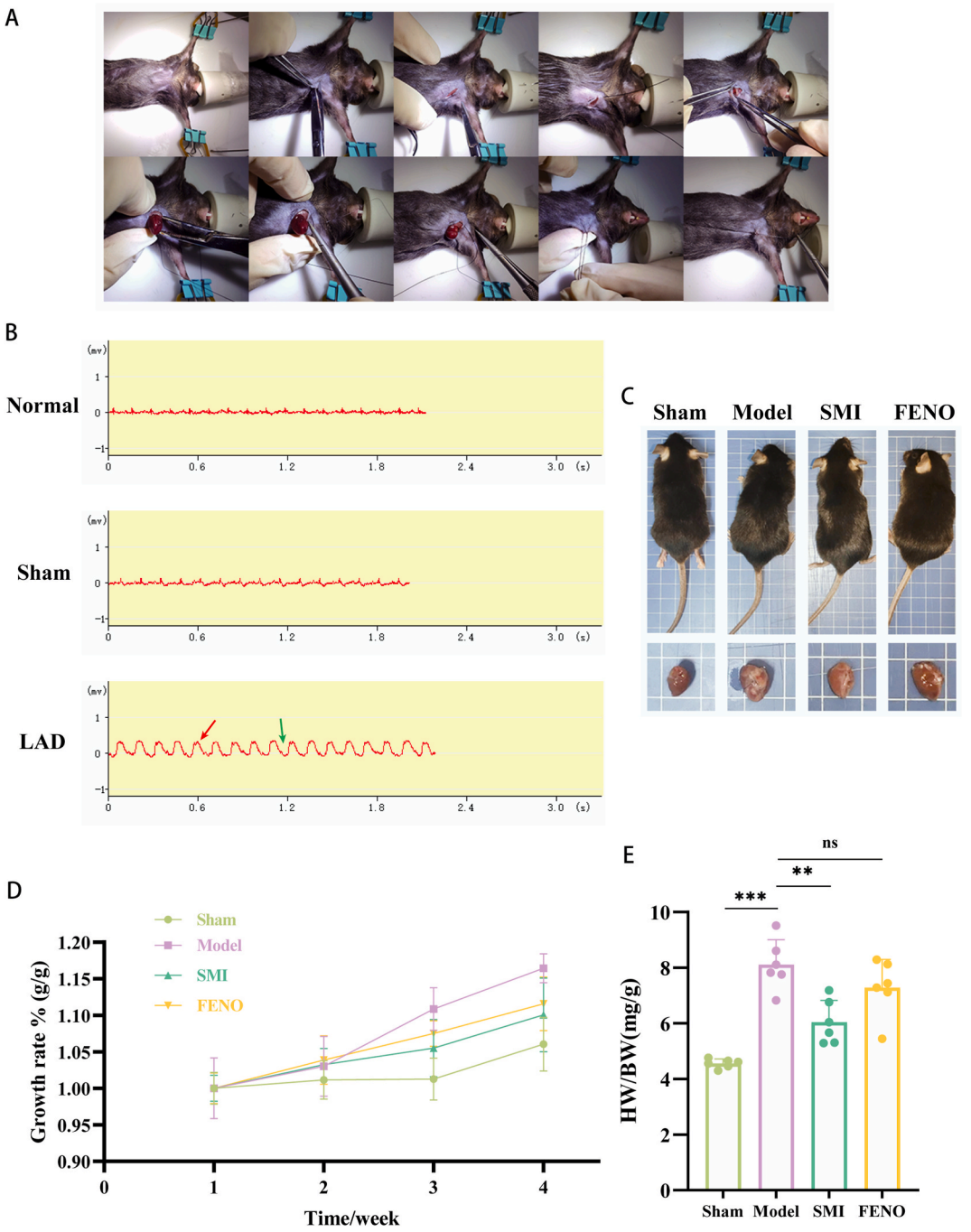

Fig. 4. Effects of SMI on electrocardiogram and body weight characteristics of mice. (A) Establishment of pMIHF model flow chart. (B) Changes in electrocardiogram before and after LAD and sham model construction. (C) Morphological changes of myocardium in each group of mice. (D) Mouse weight gain rate. (E) Heart-to-body weight ratio of mice. Results are means ± SD (n = 6), compared with model group, $^{*}P < 0.05$, $^{**}P < 0.01$, and $^{***}P < 0.001$; ns indicates no statistical significance.

3.10. Cardiac histopathological changes

The hematoxylin and eosin staining images (Fig. 6) showed that the myocardial tissue structure of the model group was disordered, characterized by fibrotic edema and infiltrated by lymphocytes and hypertrophic cells. In contrast, the myocardial cells in the SMI group were more orderly and continuous, with reduced extracellular interstitial inflammatory infiltration, and only a few inflammatory cells in the interstitium. The Masson's trichrome staining results (Fig. 6) also indicated that the extent of the lesion in the SMI

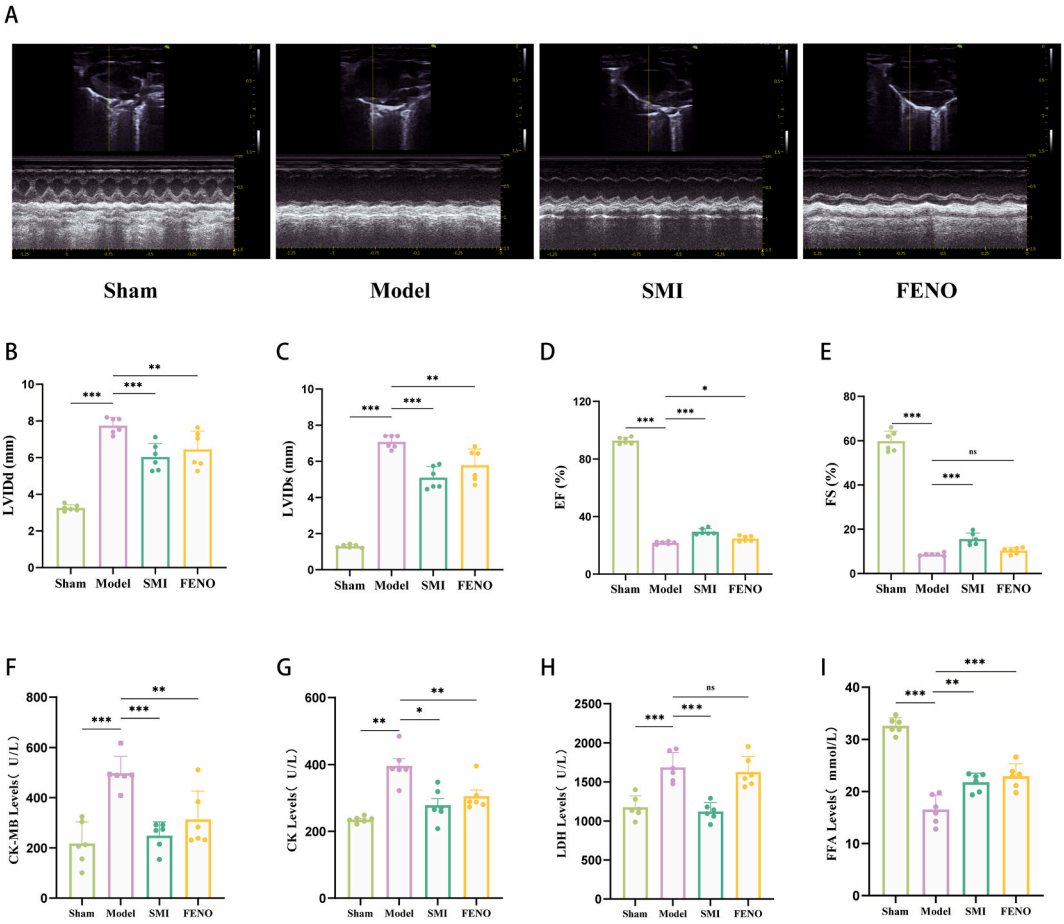

Fig. 5. Impact of SMI on cardiac function, myocardial injury marker levels, and free fatty acid (FFA) content. (A) Cardiac function of mice in each group was detected using M-mode echocardiography. Left ventricular internal dimension in (B) diastole (LVIDd) and (C) systole (LVIDs) values of mice. (D) Ejection fraction (EF) of mice. (E) Fractional shortening (FS) of mice. (F) CK-MB Content of mice. (G) CK Content of mice. (H) LDH Content of mice. (I) FFA Content of mice. Results are means ± SD, n = 6, compared with model group; $^{*}P < 0.05$, $^{**}P < 0.01$, and $^{***}P < 0.001$, ns indicates no statistical significance.

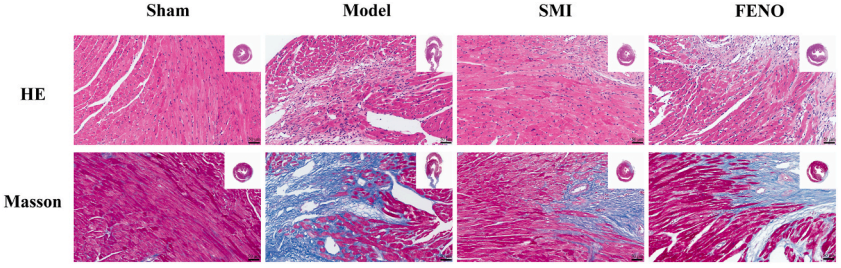

Fig. 6. Hematoxylin and eosin and Masson trichrome staining images (n = 3, scale bar: 50 μm).

group was smaller than that of the other groups and there was an improvement in the degree of myocardial fibrosis caused by collagen and fibroblasts. These findings suggest that SMI reduced inflammatory infiltration and structural remodeling in the hearts of LAD mice.

3.11. Myocardial mitochondrial electron microscopy

The electron microscopy results (Fig. 7) showed that in the sham group, the mitochondria appeared normal with a clear structure where the cristae were elongated, tightly packed, and orderly arranged, and the outer membrane was intact. In contrast, there were fewer mitochondria in the myocardial cells of the model group than in the sham group, and the mitochondria exhibited matrix swelling

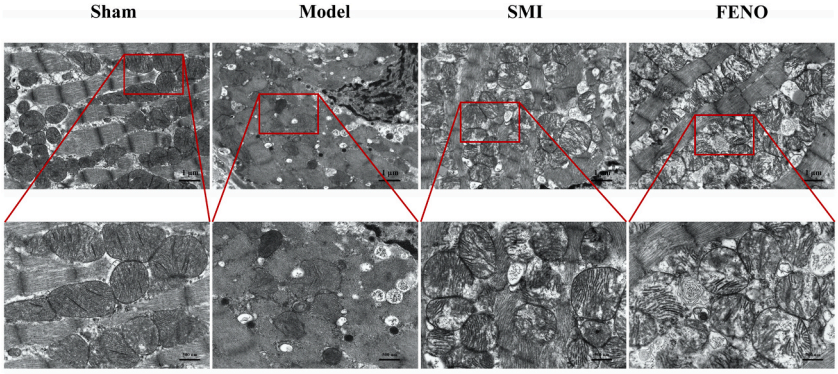

Fig. 7. Electron microscopy scanning of mouse myocardial tissues samples (n = 3, scale bar: 1 μm, 500 nm).

and vacuolation. In addition, the mitochondria were disorganized with loosely arranged cristae and the overall structure was chaotic. However, following treatment with SMI and fenofibrate, the mitochondrial structure was relatively intact, and there were more cell than there were in the model group, while the cristae appear more compact.

3.12. Impact of I/R injury on viability of H9C2 cardiomyocytes

The results of the CCK8 assay (Fig. 8A) showed that after 2 h of exposure to hypoxia followed by 1, 3, and 6 h of reoxygenation, the survival rates of cardiomyocytes decreased significantly to 74.43 %, 40.1 %, and 33.6 %, respectively, compared to that of the control group. Considering the therapeutic efficacy of drugs in hypoxic cardiomyocyte injury, we selected 2 h hypoxia followed by 3 h reoxygenation as the parameters for establishing the I/R-induced cardiomyocyte injury model.

3.13. Effect of SMI on H9C2 cardiomyocyte viability under I/R injury

The results of the assessment of the cytotoxicity of SMI on H9C2 cardiomyocytes showed that there was no significant effect on the survival rate at all concentrations tested compared with the control group (Fig. 8B). Furthermore, the CCK8 results (Fig. 8C) showed that the survival rates of the I/R injured H9C2 cardiomyocytes treated with SMI were enhanced, and the highest increase in cell survival rate of 62.46 % was observed at a concentration of 5 μl/mL. Based on these findings, we selected 5 μl/ml as the optimal concentration for SMI in subsequent experiments.

3.14. SMI enhances cardiomyocyte lipid metabolism through PPARα/SIRT1/PGC1α pathway

Further investigation of the effect of SMI on the PPARα-mediated downstream lipid oxidation pathways were focused on the mitochondrial membrane potential. The results revealed that while the control group exhibited stable mitochondrial membrane potential and strong red fluorescence signals, the I/R group showed a significant reduction in membrane potential (Fig. 9A). Notably, the I/R + SMI group exhibited an more enhanced red fluorescence signal in the mitochondria than that of the I/R group, and a relative increase in the total number of mitochondria.

The results of the RT-qPCR analysis (Fig. 9B–H) showed that PPARα expression was downregulated to 70.58 % in the I/R group compared to the control group ($P < 0.01$). Treatment with SMI significantly upregulated the expression level of PPARα compared to

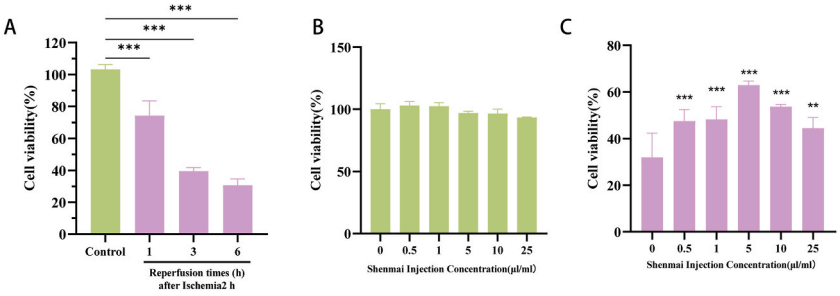

Fig. 8. Effect of SMI on H9C2 Cardiomyocyte viability. (A) Effects of different reoxygenation times on myocardial cell viability. Results are means ± SD, n = 5, compared with the control group, ***$P < 0.001$. (B) Effect of SMI on cardiomyocyte viability. Results are means ± SD, n = 5, compared with control group. (C) Effect of SMI on viability of cardiomyocytes exposed to ischemia-reperfusion injury. Results are means ± SD, n = 5, compared with control group, **$P < 0.01$, and ***$P < 0.001$.

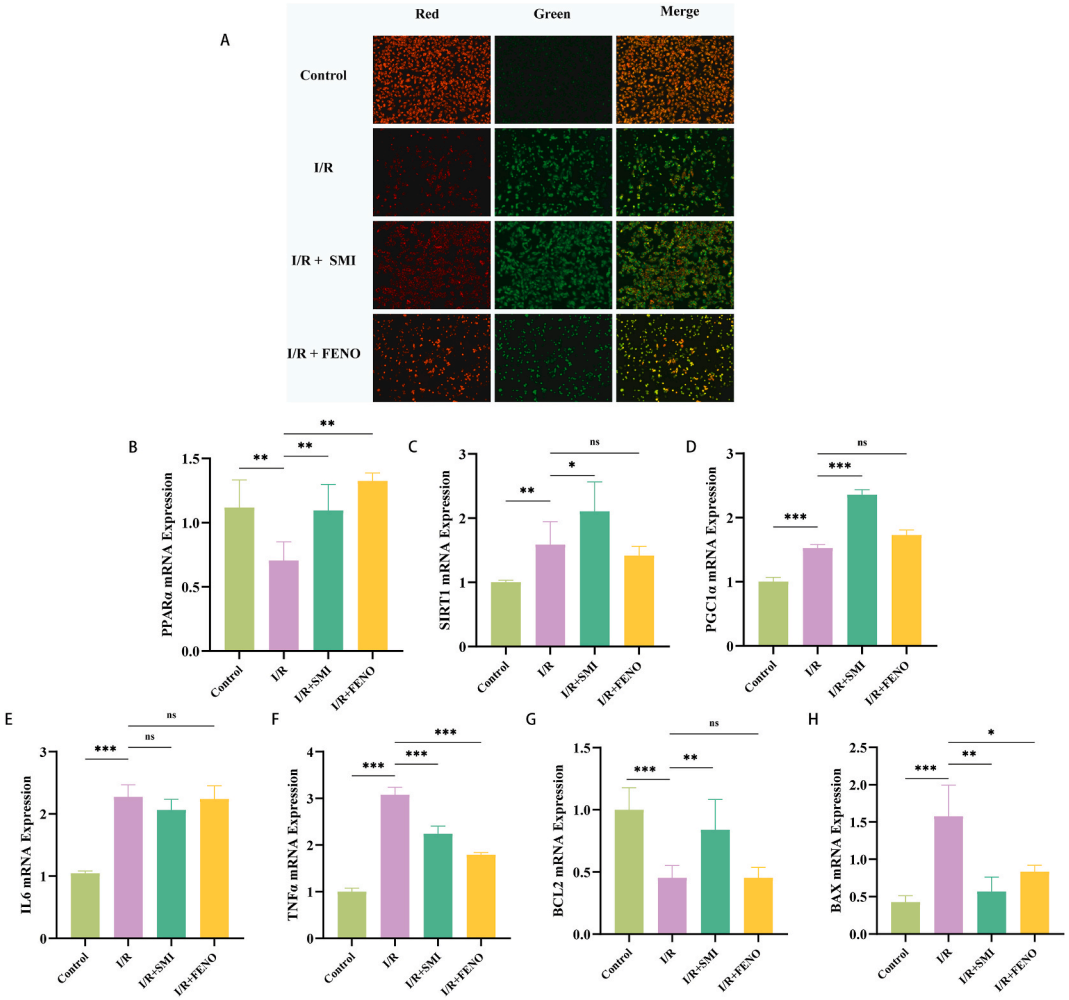

Fig. 9. Effects of SMI on mitochondrial morphology and lipid metabolism-related factors in cardiomyocytes. (A) Mitochondrial membrane potential detection. RT-qPCR analysis of PPARα (B), SIRT1 (C), PGC1α (D), IL-6 (E), TNFα (F), BCL2 (G), BAX (H). Results are means ± SD, n = 3, compared with model group; $^{*}P < 0.05$, $^{**}P < 0.01$, and $^{***}P < 0.001$, ns indicates no statistical significance.

that in the I/R group. Although the expression levels of SIRT1 and PGC1α were upregulated in the I/R group relative to the control, the effect on the cells was minimal. However, the expression levels of SIRT1 and PGC1α were increased more in the SMI-treated group than they were in the I/R group.

3.15. SMI enhances expressions of proteins in PPARα/SIRT1/PGC1α pathway

Compared to the Control group, the protein levels of PPARα, SIRT1, and PGC1α were significantly decreased in the I/R group (Fig. 10). However, in the I/R + SMI group and I/R + FENO group, the protein levels of PPARα were significantly elevated in comparison to the I/R group (Fig. 10B). Additionally, the protein levels of SIRT1 and PGC1α were notably higher in the I/R + SMI group (Fig. 10C–D). Similarly, the I/R + FENO group also experienced a significant increase in the protein levels of SIRT1 and PGC1α, although the effect was not as pronounced as with SMI.

4. Discussion

Myocardial ischemia resulting from MI will markedly alter myocardial energy metabolism. Ischemia and hypoxia will suppress the oxidative metabolism of fatty acids, carbohydrates, ketones, and amino acids, while anaerobic glycolysis will be triggered. However, the energy production efficiency of anaerobic glycolysis is considerably lower than that of lipid metabolism, leading to an insufficient energy supply and potentially resulting in heart failure [23,24]. Thus, effective regulation of lipid metabolism is crucial for improving cardiovascular diseases.

Currently, clinical treatment of heart failure relies primarily on surgical intervention and pharmacotherapy [25]. Although drugs

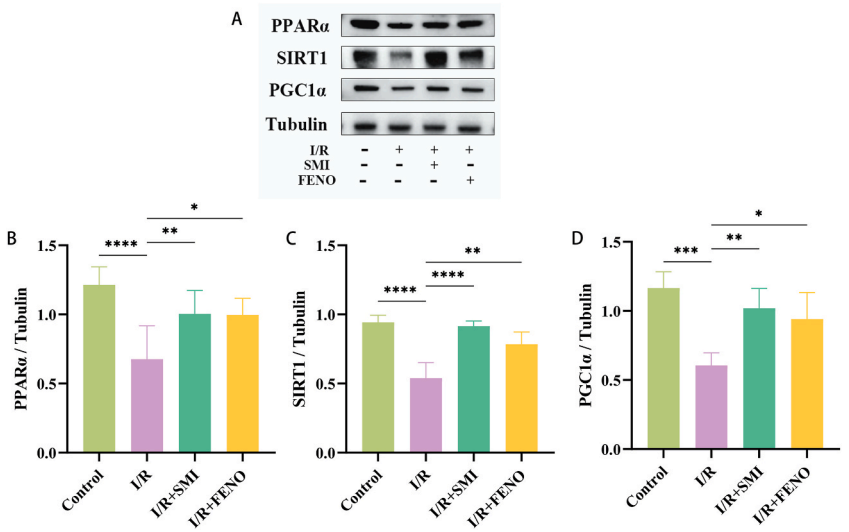

Fig. 10. The relative expression level of proteins in the PPARα/SIRT1/PGC1α pathway. (A) Protein Levels of PPARα, SIRT1, PGC1α. Quantitative analysis of PPARα (B), SIRT1 (C), PGC1α (D). Results are means ± SD, n = 3, compared with model group; $^{*}P < 0.05$, $^{**}P < 0.01$, and $^{***}P < 0.001$, ns indicates no statistical significance.

such as renin-angiotensin inhibitors [26], β-blockers [27], and statins [28] are widely used for the prevention and treatment of heart failure, they have disadvantages including slow onset of action, numerous adverse reactions, and singular activity. Moreover, surgical intervention is associated with high risk, significant costs, and poor prognosis [29,30]. In contrast, extensive clinical data indicate that traditional Chinese medicine therapies significantly improve energy metabolism during heart failure treatment, offering advantages such as minimal toxicity, notable effectiveness, and a comprehensive treatment approach [31,32]. Furthermore, traditional Chinese medicine treatments a play a significant role in the regulation of lipid metabolism during treatment [33].

In this study, we investigated the effects of SMI on lipid metabolism in pMIHF and further elucidated the associated potential mechanisms of action. To this achieved this aim, we used network pharmacology analysis to identify the primary active components and potential targets of SMI and integrated database analyses to determine the disease-related targets associated with pMIHF. This strategy identified 26 core targets, including IL6, TNF, PPARα, and SIRT1. Further analysis using GO and KEGG pathways revealed that the mechanisms of action of SMI are closely related to anti-inflammatory, anti-apoptotic, and lipid metabolism processes.

We conducted molecular docking analysis between PPARα and the most closely related effective active components in SMI to validate the accuracy of our predictions. The binding activity between PPARα and each active component of SMI was assessed based on the magnitude of the free binding energy. A binding energy > -5.0 kcal/mol is generally accepted to indicate good binding activity between the target and component. Molecular docking validation indicated that the active components of SMI exhibited strong binding activity with PPARα, suggesting that this protein might be a key therapeutic target for SMI in improving pMIHF lipid metabolism.

PPARα, a member of the peroxisome proliferator-activated receptor nuclear receptor subfamily, acts as a key transcriptional regulator in energy metabolism and plays a crucial role in myocardial fatty acid metabolism. It binds to various endogenous ligands to regulate fatty acid metabolism [34] and glucose homeostasis [35]. As a regulator of lipid metabolism, PPARα influences the expression and function of multiple related enzymes, including PGC1α, ACADL, ACADM, and CD36 molecule, functioning as a lipid sensor and central regulator [36–39]. The absence of PPARα in deficient mouse models leads to impaired fatty acid utilization and transport, highlighting its importance in cardiac function [40,41].

SIRT1, an NAD-dependent deacetylase, promotes the expression of PPARα target genes and fatty acid utilization [42], preventing myocardial hypertrophy and metabolic dysregulation [43]. Additionally, PPARα possesses anti-inflammatory and anti-apoptotic properties, making it a promising therapeutic target for myocardial I/R injury treatment [44,45].

In this study, we focused on the PPARα pathway and the therapeutic mechanisms of SMI on pMIHF using animal and cellular experiments. The echocardiographic assessment we conducted revealed that SMI effectively reduced left ventricular dysfunction in LAD mice, ameliorated the enlargement of the left ventricular diameter caused by MI, and enhanced myocardial ejection capacity, thereby improving cardiac function. Damage to myocardial cells releases intracellular components, such as aspartate aminotransferase (AST), cardiac troponin I (cTnI), CK-MB, CK, and LDH into the bloodstream [46,47]. Consequently, the severity of myocardial damage can be indirectly determined by measuring the levels of these cardiac enzymes in the peripheral serum. The results in this study indicated that MI caused severe myocardial damage with significant increases in LDH, CK, and CK-MB levels. However, treatment with SMI and fenofibrate alleviated the myocardial damage to some extent, thereby reducing the release of markers of myocardial damage. These results suggest that SMI protected the cardiac function of LAD mice. Furthermore, treatment with SMI increased serum FFA levels of the LAD mice, thereby enhancing the utilization efficiency of FFAs and improving lipid metabolism. This observation indicates that SMI reduced the expression of myocardial damage markers, thereby alleviating myocardial injury. Hematoxylin and eosin and Masson's trichome staining revealed that SMI reduce inflammatory infiltration in infarcted areas of the heart and inhibit myocardial

fibrosis, thereby decreasing myocardial structural rigidity [48]. The mitochondria are crucial for lipid metabolism and participate in the transport and oxidation of fatty acids [49].

SMI has significant effects on the regulation of myocardial lipid metabolism, although the specific mechanisms remain unclear. Studies by Ref. [50] found that SMI alleviated microvascular dysfunction by reducing levels of LDH, troponin I3, cardiac type (cTnI), endothelin-1 (ET-1), TNF-α, and IL-6, thereby improving endothelial function and microvascular structure. We also assessed both mitochondrial structure and membrane potential in vivo and in vitro, and found that SMI maintained the integrity of myocardial tissue mitochondrial morphology and inhibited mitochondrial autophagy. Furthermore, it enhanced mitochondrial membrane potential in I/R-injured myocardial cells, thus improving mitochondrial function and stabilizing lipid metabolism. The quantitative real-time polymerase chain reaction results showed that SMI significantly increased the mRNA expression of PPARα, SIRT1, and PGC1α, effectively reduced TNF-α mRNA levels, and increased BCL2 mRNA levels. Treatment with fenofibrate upregulated the expression of PPARα but that of SIRT1 was not significantly affected. Furthermore, the upregulation of PGC1α mRNA was less pronounced with fenofibrate than it was with SMI. Western Blot analysis was used to detect the protein levels of PPARα, SIRT1, and PGC1α. The results revealed a significant down-regulation of these proteins in I/R-injured cardiomyocytes compared to normal cells, suggesting damage to the lipid metabolism process. Upon treatment with SMI, there was a notable up-regulation of PPARα, SIRT1, and PGC1α proteins. Hence, SMI may regulate lipid metabolism through the coordination of PPARα and SIRT1 to modulate PGC1α.

This study has confirmed that SMI can regulate lipid metabolism in pMIHF injury through the PPARα pathway. However, there are limitations to consider. The expression and regulation of PPARα in the heart are influenced by various mechanisms, so the discussion on the synergy between PPARα and SIRT1 in this study is only a piece of the puzzle. Further research is needed to explore the upstream and downstream pathways.

5. Conclusion

In this study, we used a comprehensive strategy that combined network pharmacological analysis and experimental validation to identify the potential active components and molecular mechanisms of action of SMI in the treatment failure pMIHF. The findings of our study demonstrated that SMI is an effective agent for improving lipid metabolism in pMIHF, while PPARα serves as a potential therapeutic target for treating pMIHF.In future research, the use of PPARα antagonists for intervention comparison will be explored, as well as the development of PPARα gene knockout animal models for deeper genetic analysis.

Funding

This study was supported by the National Natural Science Foundation of China (No. 81670447), the Medicine and Health Project of Zhejiang Province (No. 2023KY531) and the Traditional Chinese Medicine Program of Zhejiang Provincial (No. 2022ZZ003, No. 2023ZL248, 2022ZB024). LW was sponsored by Ten-thousand Talents Program of Zhejiang Province (No. 2021R52025).

Data availability

All the relevant data are included in the manuscript and the supplementary document. No separate repository is attached.

CRediT authorship contribution statement

Jing Yang: Writing – original draft, Visualization, Methodology, Investigation. **Man Zhao:** Writing – review & editing, Supervision, Resources. **Ting Zeng:** Software, Methodology. **Lifang Ye:** Writing – review & editing, Resources, Conceptualization. **Yang Gui:** Methodology, Investigation. **Lihong Wang:** Writing – review & editing, Supervision, Project administration, Funding acquisition.

Declaration of competing interest

The authors declare that they have no known competing financial interests or personal relationships that could have appeared to influence the work reported in this paper.

Abbreviations

CK	Creatine Kinase
CK-MB	Creatine Kinase isoenzymes
ETCM	The Encyclopedia of Traditional Chinese Medicine
FE	Ejection Fraction
FFA	Free Fatty Acid
FS	Fractional Shortening
GO	Gene Ontology
I/R	Ischemia-Reperfusion
IL-6	Interleukin 6
KEGG	Kyoto Encyclopedia of Genes and Genomes

LDH	Lactate Dehydrogenase
LVIDd	left Ventricular Internal Diameter in diastole
LVIDs	left Ventricular Internal Diameter in systole
MI	Myocardial Infarction
PGC1α	Peroxisome proliferators-activated receptor γ coactivator 1 alpha
pMIHF	post-Myocardial Infarction Heart Failure
PPARα	Peroxisome Proliferators-ActivatedReceptor alpha
SIRT1	Silent Information Regulator 1
SMI	Shenmai Injection
TCMSP	Traditional Chinese Medicine Systems Pharmacology Database and Analysis Platform
TNFα	Tumour Necrosis Factor alpha

Appendix A. Supplementary data

Supplementary data to this article can be found online at https://doi.org/10.1016/j.heliyon.2024.e38648.

References

[1] H. Hui, X. Zhengfu, Q. Yuan, Z. Wei, Z. Chenjun, J. Mei, D. Shengqiong, W. Hairong, Exosomes from SIRT1-overexpressing ADSCs restore cardiac function by improving the angiogenic functions of EPCs, Mol. Ther. Nucleic Acids 21 (2020) 737–750, https://doi.org/10.1016/j.omtn.2020.07.007.

[2] Y. Xie, H. Zhang, T. Huang, Quantitative proteomics reveal three potential biomarkers for risk assessment of acute myocardial infarction, Bioengineered 13 (2022) 4939–4950, https://doi.org/10.1080/21655979.2022.2037365.

[3] W. Yao, H. Mengying, D. Shanzhou, Z. Zhiwen, W. Xuejie, C. Yongbing, Y. Lichen, Macrophage-targeting gene silencing orchestrates myocardial microenvironment remodeling toward the anti-inflammatory treatment of ischemia-reperfusion (IR) injury, Bioact. Mater. 17 (0) (2022) 320–333, https://doi.org/10.1016/j.bioactmat.2022.01.026.

[4] X.M. Caravia, V. Fanjul, E. Oliver, D. Roiz-Valle, A. Morán-Álvarez, G. Desdín-Micó, M. Mittelbrunn, R. Cabo, J.A. Vega, F. Rodríguez, A. Fueyo, M. Gómez, M. Lobo-González, H. Bueno, G. Velasco, J.M.P. Freije, V. Andrés, B. Ibáñez, A.P. Ugalde, C. López-Otín, The microRNA-29/PGC1α regulatory axis is critical for metabolic control of cardiac function, PLoS Biol. 16 (2018) e2006247, https://doi.org/10.1371/journal.pbio.2006247.

[5] L.D. Zorova, V.A. Popkov, E.Y. Plotnikov, D.N. Silachev, I.B. Pevzner, S.S. Jankauskas, V.A. Babenko, S.D. Zorov, A.V. Balakireva, M. Juhaszova, S.J. Sollott, D. B. Zorov, Mitochondrial membrane potential, Anal. Biochem. 552 (2018) 50–59, https://doi.org/10.1016/j.ab.2017.07.009.

[6] Y. Wang, Q. Liu, Y. Kong, G. Zhong, D. Wang, Efficacy and safety evaluation of Shenmai injections for dilated cardiomyopathy: a systematic review and meta-analysis of randomised controlled trials, Phytomedicine 110 (2023) 154630, https://doi.org/10.1016/j.phymed.2022.154630.

[7] W.Y. Liu, J.W. Zhang, X.Q. Yao, C. Jiang, J.C. He, P. Ni, J.L. Liu, Q.Y. Chen, Q.R. Li, X.J. Zang, L. Yao, Y.Z. Liu, M.L. Wang, P.Q. Shen, G.J. Wang, F. Zhou, Shenmai injection enhanced the cytotoxicity of chemotherapeutic drugs against colorectal cancers by improving their subcellular distribution, Acta Pharmacol. Sin. 38 (2017) 264–276, https://doi.org/10.1038/aps.2016.99.

[8] P. Zhou, G. Gao, C.C. Zhao, J.Y. Li, J.F. Peng, S.S. Wang, R. Song, H. Shi, L. Wang, In vivo and in vitro protective effects of shengmai injection against doxorubicin-induced cardiotoxicity, Pharm. Biol. 60 (2022) 638–651, https://doi.org/10.1080/13880209.2022.2046801.

[9] S. Wang, L. Ye, L. Wang, Protective mechanism of Shenmai in myocardial ischemia/reperfusion through energy metabolism pathway, Am. J. Transl. Res. 11 (2019) 4046–4062.

[10] S.M. Wang, L.F. Ye, L.H. Wang, Shenmai injection improves energy metabolism in patients with heart failure: a randomized controlled trial, Front. Pharmacol. 11 (2020) 459, https://doi.org/10.3389/fphar.2020.00459.

[11] Z. Wu, W. Li, G. Liu, Y. Tang, Network-based methods for prediction of drug-target interactions, Front. Pharmacol. 9 (2018) 1134, https://doi.org/10.3389/fphar.2018.01134.

[12] R. Jinlong, L. Peng, W. Jinan, L. Bohui, H. Chao, L. Pidong, G. Zihu, T. Weiyang, Y. Yinfeng, X. Xu, L. Yan, W. Yonghua, Y. Ling, TCMSP: a database of systems pharmacology for drug discovery in herbal medicines, J. Cheminform. 6 (1) (2014), https://doi.org/10.1186/1758-2946-6-13.

[13] X. Haiyu, Z. Yanqiong, L. Zhenming, C. Tong, L. Chuanyu, T. Shihuan, Z. Xiaobo, Z. Wei, L. Zhiyong, Z. Rongrong, Y. Hongjun, W. Xiujie, H. Luqi, ETCM: an encyclopaedia of traditional Chinese medicine, Nucleic Acids Res. 47 (D1) (2018) D976–D982, https://doi.org/10.1093/nar/gky987.

[14] D. Antoine, M. Olivier, Z. Vincent, SwissADME: a free web tool to evaluate the pharmacokinetics, drug-likeness, and medicinal chemistry friendliness of small molecules, Sci. Rep. 7 (2017) 42717, https://doi.org/10.1038/srep42717.

[15] J. Piñero, J.M. Ramírez-Angenia, J. Saüch-Pitarch, F. Ronzano, E. Centeno, F. Sanz, L.I. Furlong, DisGeNET knowledge platform for disease genomics: 2019 update, Nucleic Acids Res. 48 (2020) D845–D855, https://doi.org/10.1093/nar/gkz1021.

[16] G. Stelzer, N. Rosen, I. Plaschkes, S. Zimmerman, M. Twik, S. Fishilevich, T.I. Stein, R. Nudel, I. Lieder, Y. Mazor, S. Kaplan, D. Dahary, D. Warshawsky, Y. Guan-Golan, A. Kohn, N. Rappaport, M. Safran, D. Lancet, GeneCards suite: from gene data mining to disease genome sequence analysis, Curr. Protoc. Bioinformatics 54 (1.30) (2016), https://doi.org/10.1002/cpbi.5, 1–1.30.33.

[17] A. Jia, L. Xu, Y. Wang, Bioinformatics Venn diagrams in bioinformatics, Brief. Bioinform. 22 (2021), https://doi.org/10.1093/bib/bbab108.

[18] D. Szklarczyk, A. Franceschini, S. Wyder, K. Forslund, D. Heller, J. Huerta-Cepas, M. Simonovic, A. Roth, A. Santos, K.P. Tsafou, M. Kuhn, P. Bork, L.J. Jensen, C. von Mering, STRING v10: protein-protein interaction networks integrated over the tree of life, Nucleic Acids Res. 43 (2015) D447–D452, https://doi.org/10.1093/nar/gku1003.

[19] T.S. Brad, M. Hao, Q. Ju, J. Xiaoli, B.H. Michael, L. Clifford, I. Tomozumi, C. Weizhong, David: a web server for functional enrichment analysis and functional annotation of gene lists (2021 updates), Nucleic Acids Res. 50 (W1) (2022) W216–W221, https://doi.org/10.1093/nar/gkac194.

[20] G. Erhe, L. Yong, S. Xianwen, H. Z Maggie, Z. Li, B. Matthieu, F. Qingyu, C. J Kurt, L. Xin, J.K. Walter, A novel and efficient model of coronary artery ligation in the mouse, Methods Mol. Biol. 1037 (2013) 299–311, https://doi.org/10.1161/circresaha.110.223925.

[21] L. Lin, L. Jinghao, W. Qilong, Z. Xin, Y. Dongli, N. Lu, Y. Yanze, Z. Xianxian, H. Limin, L. Yuhong, Shenmai injection protects against DOX-induced cardiotoxicity by maintaining mitochondrial homeostasis, Front. Pharmacol. 11 (2020) 815, https://doi.org/10.3389/fphar.2020.00815.

[22] Z. Qian, H. Guizhen, W. Jie, W. Yukang, C. Wei, Protective effects of fenofibrate against intestinal ischemia/reperfusion in mice, Sci. Rep. 6 (1) (2016), https://doi.org/10.1038/srep22044.

[23] H. Jun, S. Ryong, S. Lae, Y. Hyun, L. Hyewon, H. Euiju, Letrozole accelerates metabolic remodeling by activating glycolysis in cardiomyocytes, a role beyond hormone regulation, Int. J. Mol. Sci. 23 (1) (2022) 547, https://doi.org/10.3390/ijms23010547.

[24] H. Ying, S. Weiju, R. Di, Z. Jingwen, H. Zhibin, F. Julia, S. Xiaodong, H. Fang, L. Ji, SIRT1 agonism modulates cardiac NLRP3 inflammasome through pyruvate dehydrogenase during ischemia and reperfusion, Redox Biol. 34 (0) (2020) 101538, https://doi.org/10.1016/j.redox.2020.101538, 101538.

[25] B. Bozkurt, Contemporary pharmacological treatments and management of heart failure, Nat. Rev. Cardiol. (2024), https://doi.org/10.1038/s41569-024-00997-0.
[26] G. Savarese, U. Dahlström, P. Vasko, B. Pitt, L.H. Lund, Association between renin and angiotensin system inhibitor use and mortality/morbidity in elderly patients with heart failure and reduced ejection fraction: a prospective propensity score-matched cohort study, Eur. Heart J. 39 (2018) 4257–4265, https://doi.org/10.1093/eurheartj/ehy621.
[27] M. Kampamba, P. Mweetwa, W. Mufwambi, A. Hamachila, J. Hangoma, Utilization and optimization of beta-adrenergic receptor blockers over a 6-month period in patients with chronic heart failure and reduced ejection fraction, S. Afr. Med. J. 113 (2023) 25–29, https://doi.org/10.7196/SAMJ.2023.v113i9.784.
[28] H. Li, Y. Wang, J. Liu, X. Chen, Y. Duan, X. Wang, Y. Shen, Y. Kuang, T. Zhuang, B. Tomlinson, P. Chan, Z. Yu, Y. Cheng, L. Zhang, Z. Liu, Y. Zhang, Z. Zhao, Q. Zhang, J. Liu, Endothelial Klf2-Foxp1-TGFβ signal mediates the inhibitory effects of simvastatin on maladaptive cardiac remodeling, Theranostics 11 (2021) 1609–1625, https://doi.org/10.7150/thno.48153.
[29] A.A. Kammerlander, C. Nitsche, C. Donà, M. Koschutnik, V. Dannenberg, K. Mascherbauer, R. Schönbauer, A. Zafar, M.P. Winter, P.E. Bartko, G. Goliasch, C. Hengstenberg, J. Mascherbauer, Heart failure with preserved ejection fraction after left-sided valve surgery: prevalence and relevance, Eur. J. Heart Fail. 23 (2021) 2008–2016, https://doi.org/10.1002/ejhf.2345.
[30] D. Shay, P.Y. Ng, D.M. Dudzinski, S.D. Grabitz, J.D. Mitchell, X. Xu, T.T. Houle, D.L. Bhatt, M. Eikermann, Preoperative heart failure treatment prevents postoperative cardiac complications in patients at lower risk: a retrospective cohort study, Ann. Surg. 277 (2023) e33–e39, https://doi.org/10.1097/SLA.0000000000004779.
[31] L. Yen, T. Jowsey, I.S. Mcrae, Consultations with complementary and alternative medicine practitioners by older Australians: results from a national survey, BMC Complement. Altern. Med. 13 (2013) 73, https://doi.org/10.1186/1472-6882-13-73.
[32] A. Tachjian, V. Maria, A. Jahangir, Use of herbal products and potential interactions in patients with cardiovascular diseases, J. Am. Coll. Cardiol. 55 (2010) 515–525, https://doi.org/10.1016/j.jacc.2009.07.074.
[33] W. Wang, H. Li, Y. Shi, J. Zhou, G.J. Khan, J. Zhu, F. Liu, H. Duan, L. Li, K. Zhai, Targeted intervention of natural medicinal active ingredients and traditional Chinese medicine on epigenetic modification: possible strategies for prevention and treatment of atherosclerosis, Phytomedicine 122 (2024) 155139, https://doi.org/10.1016/j.phymed.2023.155139.
[34] N. Bougarne, B. Weyers, S.J. Desmet, J. Deckers, D.W. Ray, B. Staels, K. De Bosscher, Molecular actions of PPARα in lipid metabolism and inflammation, Endocr. Rev. 39 (2018) 760–802, https://doi.org/10.1210/er.2018-00064.
[35] P. Hu, K. Li, X. Peng, Y. Kan, H. Li, Y. Zhu, Z. Wang, Z. Li, H.Y. Liu, D. Cai, Nuclear receptor PPARα as a therapeutic target in diseases associated with lipid metabolism disorders, Nutrients 15 (2023) 4772, https://doi.org/10.3390/nu15224772.
[36] Y. Angen, X. Yi-Chuang, H. Christer, Z. Tao, T. Xiaoying, W. Xiaolei, S. Yong, L. Zhi, Klf4-Sirt3/Pparα-Lcad pathway contributes to high phosphate-induced lipid degradation, Cell Commun. Signal. 21 (1) (2023) 5, https://doi.org/10.1186/s12964-022-01008-w.
[37] L. Du, H. Lu, Z. Wang, C. Liu, Y. Xiao, Z. Guo, Y. Li, Therapeutic potential of ginsenoside Rb1-PLGA nanoparticles for heart failure treatment via the ROS/PPARα/PGC1α pathway, Molecules 28 (2023) 8118, https://doi.org/10.3390/molecules28248118.
[38] S. Kazuharu, S. Goki, Y. Yoshiya, F. Ken, B. Masaru, N. Akinobu, M. Hideaki, K. Megumi, M. Osamu, Y. Ryoichi, K. Takashi, Y. Koji, S. Taku, N. Akihisa, O. Masatsugu, K. Naoki, N. Masato, S. Takuya, N. Mitsuteru, M. Kenichi, O. Koji, O. Shunsuke, Sakamoto Naoya, Tenofovir–disoproxil–fumarate modulates lipid metabolism via hepatic CD36/PPAR-alpha activation in hepatitis B virus infection, J. Gastroenterol. 56 (2) (2020) 168–180, https://doi.org/10.1007/s00535-020-01750-3.
[39] Shipra, M.K. Tembhre, M.P. Hote, N. Bhari, R. Lakshmy, S.S. Kumaran, PGC-1α agonist rescues doxorubicin-induced cardiomyopathy by mitigating the oxidative stress and necroptosis, Antioxidants 12 (2023), https://doi.org/10.3390/antiox12091720.
[40] P.J. Smeets, B.E. Teunissen, P.H. Willemsen, F.A. van Nieuwenhoven, A.E. Brouns, B.J. Janssen, J.P. Cleutjens, B. Staels, G.J. van der Vusse, M. van Bilsen, Cardiac hypertrophy is enhanced in PPARα-/- mice in response to chronic pressure overload, Cardiovasc. Res. 78 (2008) 79–89, https://doi.org/10.1093/cvr/cvn001.
[41] Z. Yemin, L. Mingxin, T. Zhao You, W. Changhua, Wogonin suppresses osteopontin expression in adipocytes by activating PPARα, Acta Pharmacol. Sin. 36 (8) (2015) 987–997, https://doi.org/10.1038/aps.2015.37.
[42] N. Mahdis Rahimi, S. Beydolah, A. Shahrzad, S. Bentolhoda, N. Mahdieh, Trehalose-induced SIRT1/AMPK activation regulates SREBP-1c/PPAR-α to alleviate lipid accumulation in aged liver, Naunyn-Schmiedeberg's Arch. Pharmacol. 397 (2) (2023) 1061–1070, https://doi.org/10.1007/s00210-023-02644-w.
[43] C. Yukai, H. Yi-Xiang, W. Wei-Yin, H. Weimin, W. Yao, W. Chan, L. Guirong, W. Yan, Acacetin ameliorates cardiac hypertrophy by activating Sirt1/AMPK/PGC-1α pathway, Eur. J. Pharmacol. 920 (0) (2022) 174858, https://doi.org/10.1016/j.ejphar.2022.174858, 174858.
[44] T. Aspasia, A. Daskalopoulou, P.D. Ilias, K. Panagiotis, A. Asier, M. Angeliki, M. Georgios, A. Leonidas G, Perrea Despoina, PPAR-alpha independent anti-inflammatory effects of fenofibrate in a transgenic model of atherosclerosis, Atherosclerosis 275 (0) (2018) e117–e118, https://doi.org/10.1016/j.atherosclerosis.2018.06.333.
[45] S. Rana, R. Datta, R.D. Chaudhuri, E. Chatterjee, M. Chawla-Sarkar, S. Sarkar, Nanotized PPARα overexpression targeted to hypertrophied myocardium improves cardiac function by attenuating the p53-GSK3β-mediated mitochondrial death pathway, Antioxid. Redox Signal. 30 (2019) 713–732, https://doi.org/10.1089/ars.2017.7371.
[46] X. Wang, W. Qin, X. Qiu, J. Cao, D. Liu, B. Sun, A novel role of exogenous carbon monoxide on protecting cardiac function and improving survival against sepsis via mitochondrial energetic metabolism pathway, Int. J. Biol. Sci. 10 (2014) 777–788, https://doi.org/10.7150/ijbs.9220.
[47] Y. Wang, Z. Guo, L. Huang, Value of different biochemical markers in early diagnosis of acute myocardial infarction, Nan Fang Yi Ke Da Xue Xue Bao 34 (2014) 1347–1350.
[48] J.T. Chiang, K.F. Badrealam, M.A. Shibu, C.H. Kuo, C.Y. Huang, B.C. Chen, Y.M. Lin, V.P. Viswanadha, W.W. Kuo, C.Y. Huang, Eriobotrya japonica ameliorates cardiac hypertrophy in H9c2 cardiomyoblasts and spontaneously hypertensive rats, Environ. Toxicol. 33 (2018) 1113–1122, https://doi.org/10.1002/tox.22589.
[49] S. Ranjbarvaziri, K.B. Kooiker, M. Ellenberger, G. Fajardo, M. Zhao, A.S. Vander Roest, R.A. Woldeyes, T.T. Koyano, R. Fong, N. Ma, L. Tian, G.M. Traber, F. Chan, J. Perrino, S. Reddy, W. Chiu, J.C. Wu, J.Y. Woo, K.M. Ruppel, J.A. Spudich, M.P. Snyder, K. Contrepois, D. Bernstein, Altered cardiac energetics and mitochondrial dysfunction in hypertrophic cardiomyopathy, Circulation 144 (2021) 1714–1731, https://doi.org/10.1161/CIRCULATIONAHA.121.053575.
[50] Z. Zheng, Z. Yu, B. Xu, Y. Zhou, Y. Xing, Q. Li, W. Tang, F. Peng, Pretreatment with shenmai injection protects against coronary microvascular dysfunction, Evid. Based Complement. Alternat. Med. 2022 (2022) 8630480, https://doi.org/10.1155/2022/8630480.